



INTERNATIONAL ATOMIC ENERGY AGENCY
UNITED NATIONS EDUCATIONAL, SCIENTIFIC AND CULTURAL ORGANIZATION
INTERNATIONAL CENTRE FOR THEORETICAL PHYSICS
I.C.T.P., P.O. BOX 586, 34100 TRIESTE, ITALY, CABLE: CENTRATOM TRIESTE



H4-SMR 1012 - 39

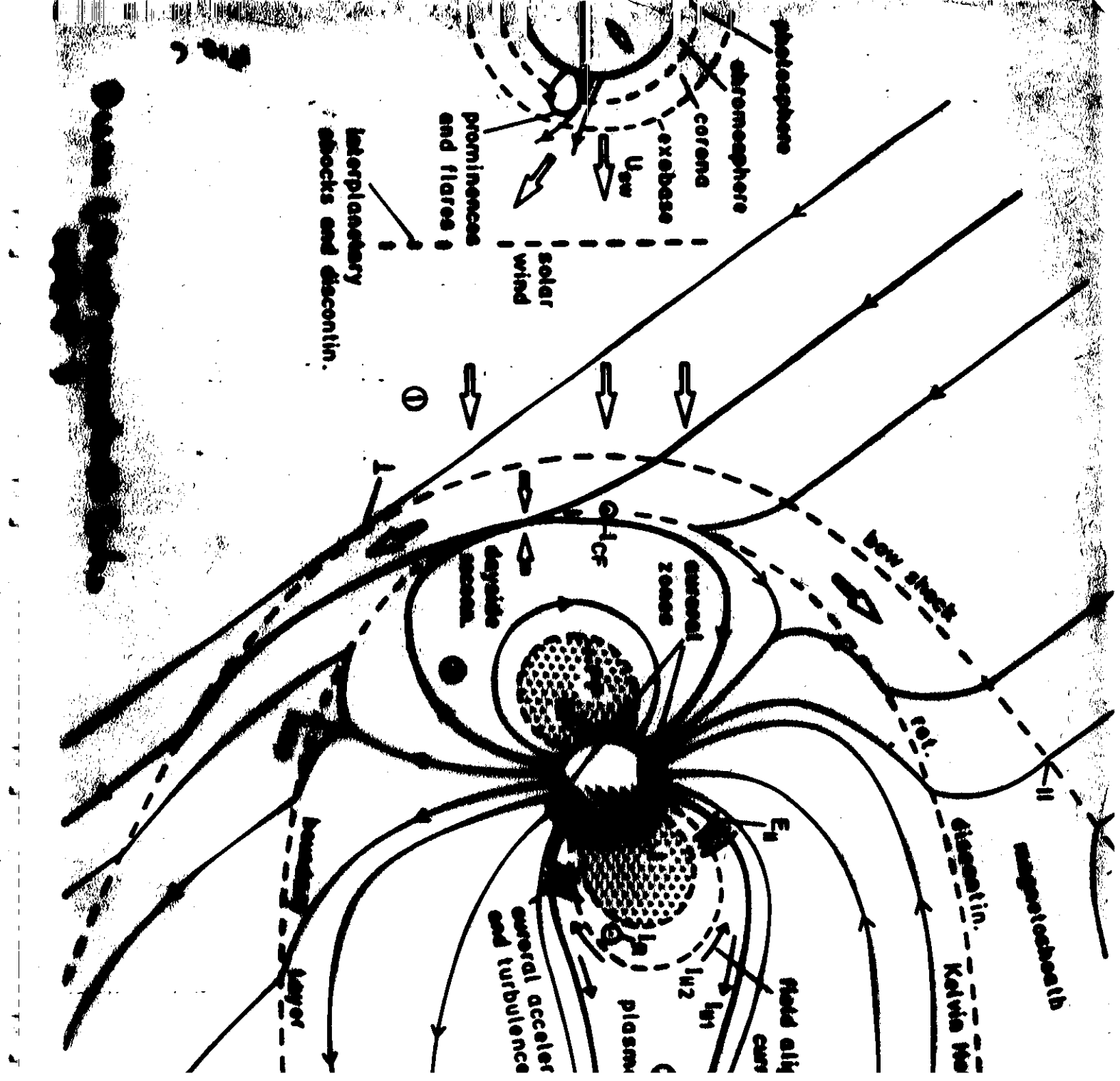
AUTUMN COLLEGE ON PLASMA PHYSICS

13 October - 7 November 1997

LECTURE NOTES (3rd set)

C.T. DUM

Max Planck Institut für Extraterrestrial Physik,
Garching, Germany



Beam-plasma interaction in a magnetic field: theory and simulation

C. T. Dum, M.P.E Garching &
M.I.T Cambridge, U.S.A

Observations: Auroral Acceleration

Precipitating electrons (beam)

~ keV

cold ionospheric plasma ~ 0.5 eV
 O^+, H^+, He^+

Auroral hiss $\omega > \omega_{LH} = \frac{\omega_i}{[1 + \omega_e^2/\omega_i^2]^{1/2}}$
cutoff

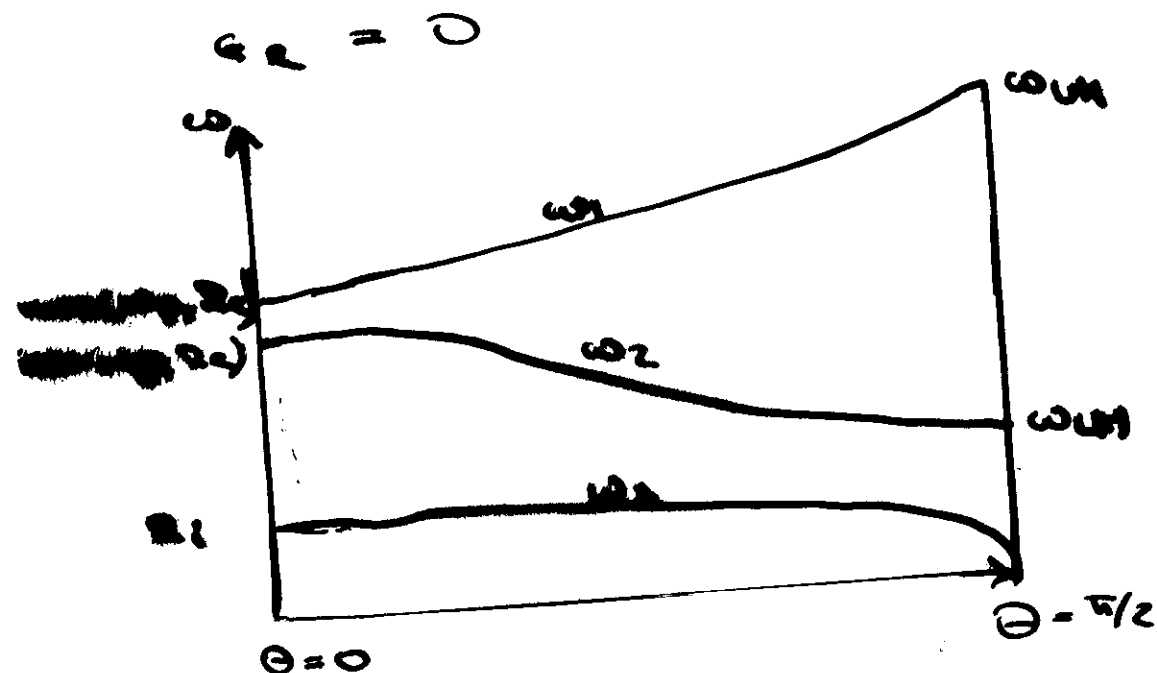
transverse ion heating

magnetic mirror force $F = -j_B \nabla B$

upward acceleration, ion conic
 $v_{\perp B} \propto B(v_{\parallel B})$ O^+ (tails)

Cold Plasma Resonances

$$\epsilon_R = 1 - \frac{\omega_p^2(\omega^2 - \Omega_e \Omega_{i1})}{(\omega^2 - \Omega_e^2)(\omega^2 - \Omega_{i1}^2)} \sin^2 \Theta - \frac{\omega_p^2}{\omega^2} \omega^2 \Theta$$



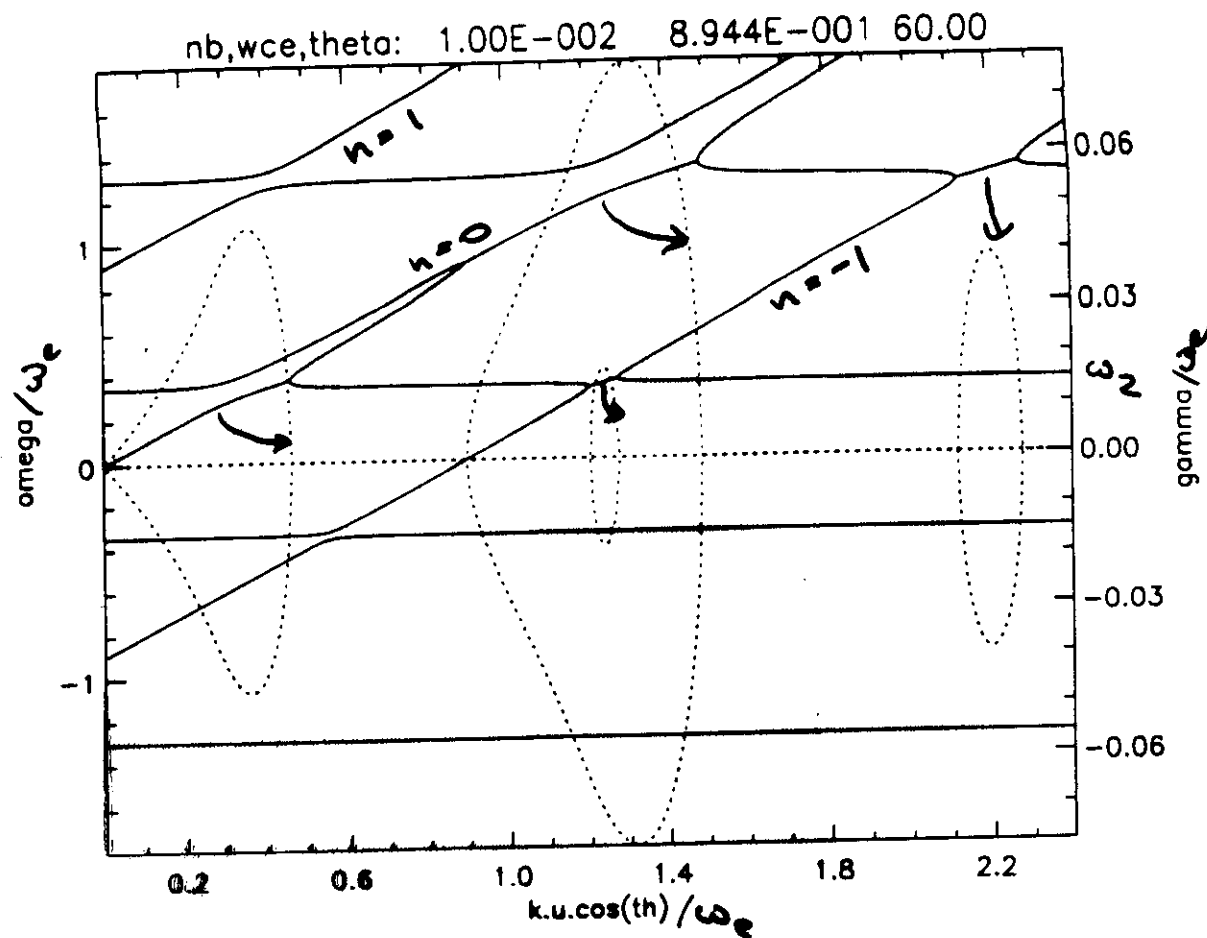
small Θ :

$$\omega_1^2 \propto \omega_p^2 + \frac{\omega_p^2 \Omega_e^2}{\omega_p^2 - \Omega_e^2} \sin^2 \Theta$$

$$\omega_2^2 \propto \omega_p^2 - \frac{\omega_p^2 \Omega_e^2}{\omega_p^2 - \Omega_e^2} \sin^2 \Theta$$

$$\omega_p > \Omega_e$$

$$\Omega_e \ll \omega_p$$



dispersion relation for
 a cold plasma and a cold
 drifting beam $n_b/n = 0.01$
 $\gamma_{ce}/\omega_e = 0.8944$
 $\approx 0^\circ$ to

Beam Driven Hybrid Waves and Anomalous Doppler Effect

C. T. DUM*

*Max-Planck-Institut für extraterrestrische Physik
P.O.Box 1603, 85740 Garching, Germany*

- **Observations:** Auroral electron beam → auroral hiss; ion conics, double streaming electrons.
transverse ion acceleration
longitudinal electron acceleration
- **Auroral hiss** $M_{De}[\omega_e, \Omega_e] > \omega > \omega_{LH} = \frac{\omega_e}{\sqrt{1 + (\omega_e/\Omega_e)^2}}$
~~unmagnetized beam, magnetized electrons~~
- **Linear instability theory:**
 - a.) Landau resonance: $\omega - k_{\parallel} v_{\parallel} = 0$ ~~$\frac{\partial f}{\partial v_{\parallel}} > 0$~~ ; beam
 - b.) Anomalous Doppler effect: $\omega - k_{\parallel} v_{\parallel} - n\Omega_E = 0$; $n = -1, -2, \dots, \frac{\partial f}{\partial v_{\perp}} < 0$ (elongated tail).
- **Quasilinear theory:** 2 stages
 - a.) Landau: Beam → plateau $\frac{\partial f}{\partial v_{\parallel}} \approx 0$
 - b.) Anom. Doppler: isotropization

Anomalous Doppler interaction

$$\omega - k_u v_u - n \Sigma_e = 0$$

$n=0$ Landau

$n=-1, -2$ Anom. Doppler

$n=1, 2$ Doppler

$$-\text{Im} \epsilon_j = \pi \frac{\omega_j^2}{k^2} \int d\mathbf{v}_\perp J_n^2 \left(\frac{k_\perp v_\perp}{\omega} \right) \frac{1}{|k_\parallel|} \times$$

$$\left[n \Sigma_e \underbrace{\frac{1}{j v_\perp} \frac{\partial S}{\partial v_\perp}}_{AD} + k_\perp \frac{\partial f}{\partial v_\parallel} \right]$$

$$v_u = \frac{\omega + \Sigma_e}{k_u}$$

need elongated tail

Fusion: electron runaway

Kondratenko, Pogutse 1967

Shugiro Shevchenko 1968

Omelchenko et al 1994 for instab.



.. - .. - ..

G1.8,nb0.02,u16,Tb3.33,ob0.36To2.0,Th2.0,nh0.1

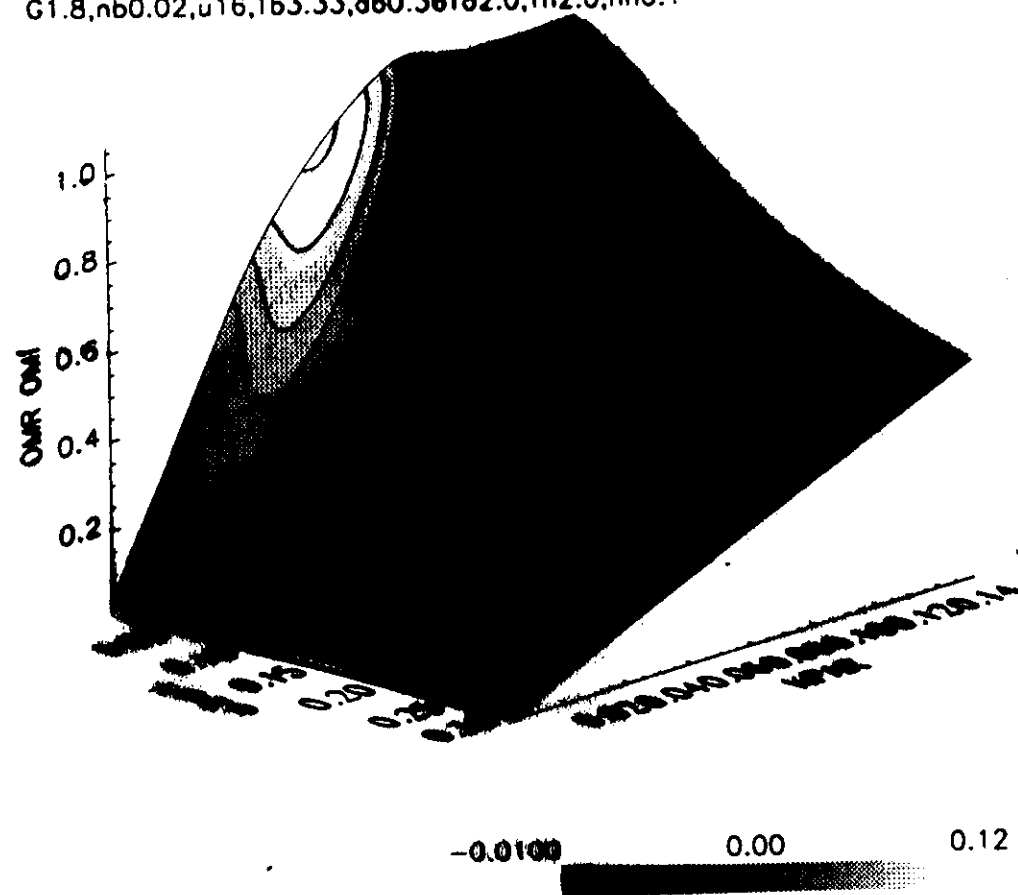
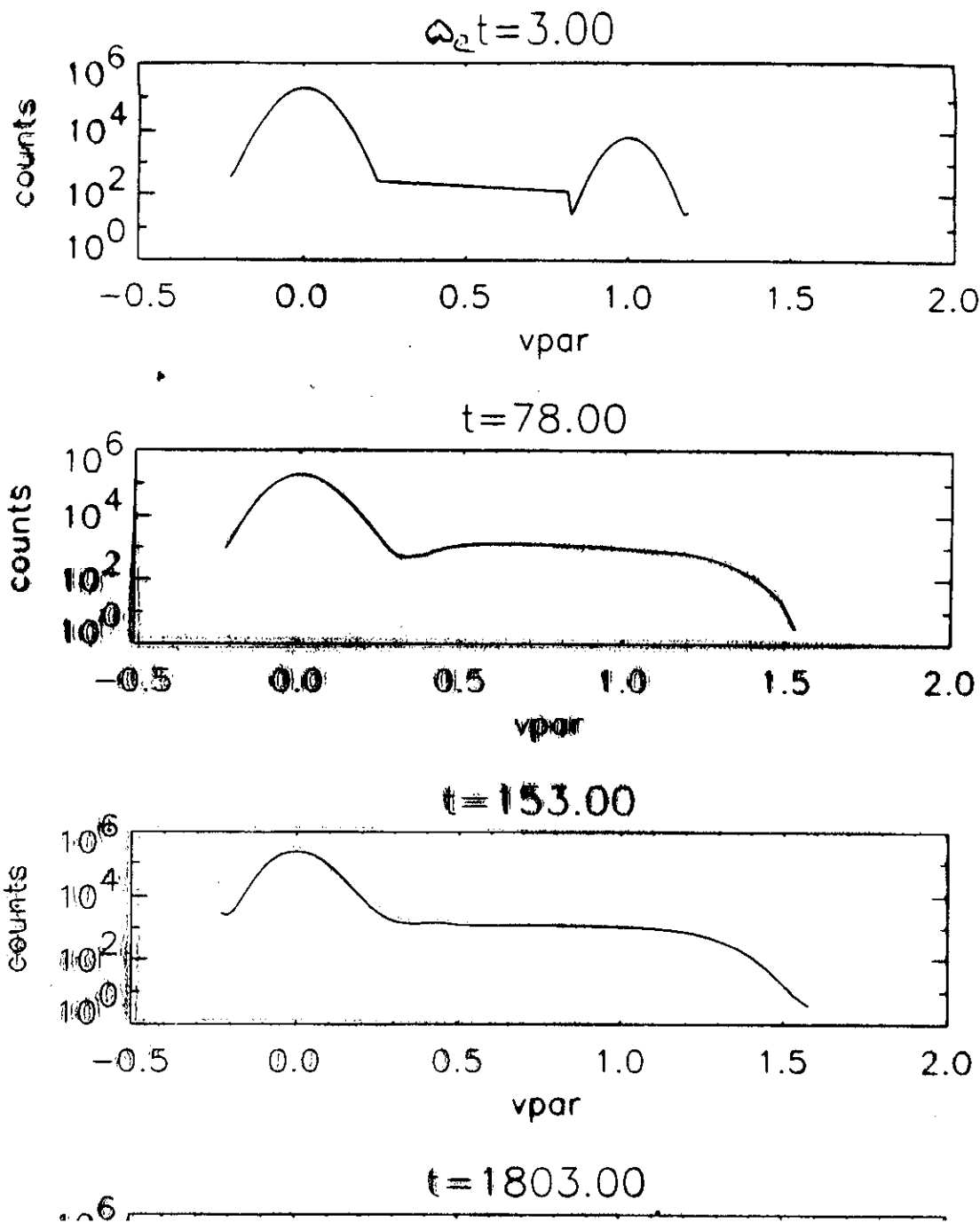


Fig. 1: Normal frequency ω/ω_e and growth rate (contours and shades) for a beam with relative density $n_b/n = 0.02$, drift $u/v_e = 16$ and $T_b/T_e = 3.33$ in an Oxygen-Hydrogen Plasma ($n_H/n = 0.1$) with $\Omega_p/\omega_e = 1.8$. The wave numbers are normalized to the electron



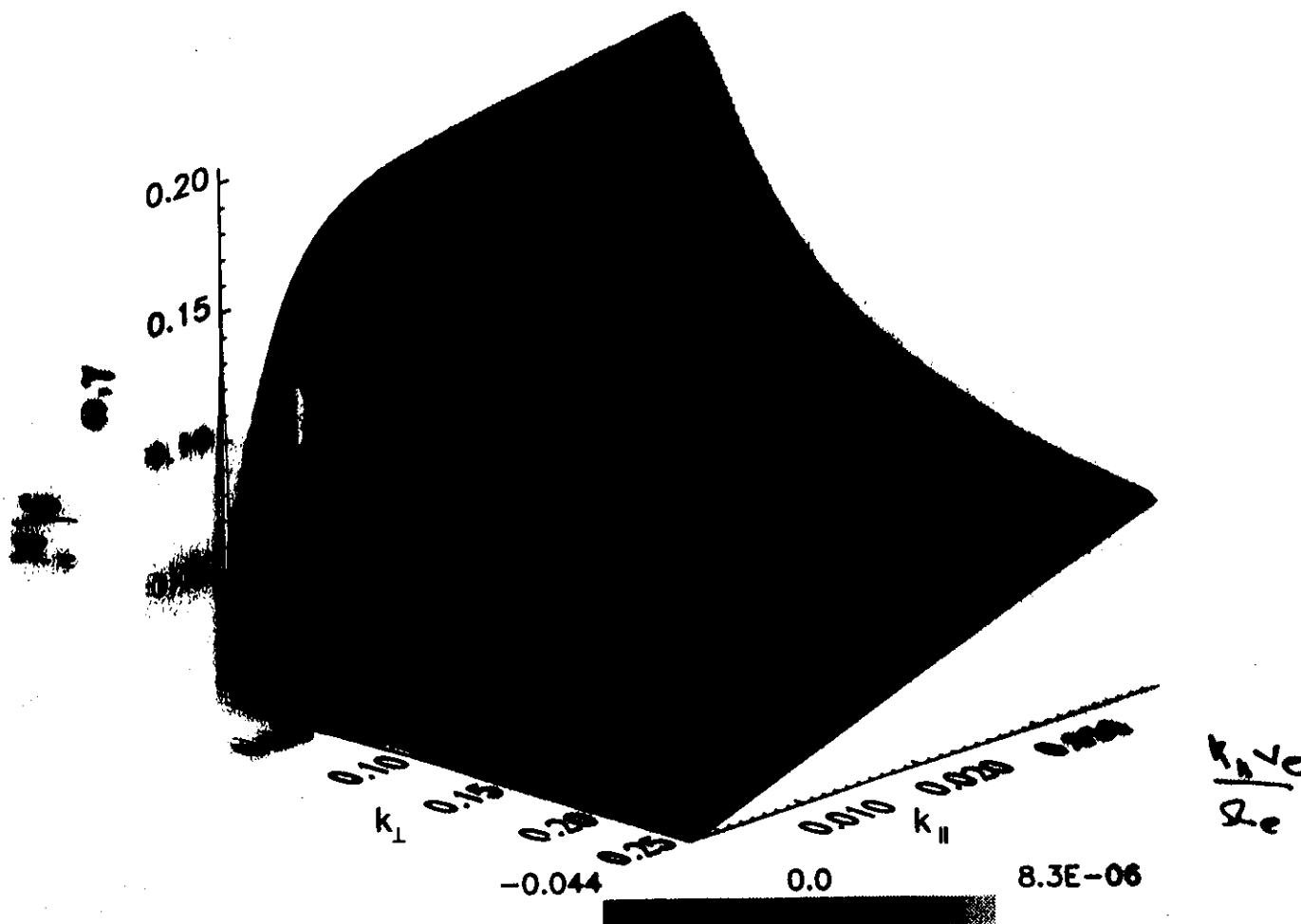


Fig. 3. a. Dispersion relation for an oxygen-hydrogen plasma with $\alpha_{O^+}/\alpha_{H^+} = 0.1945$, $n_H/n_e = 0.1$ and a flat topped beam with $n_b/n = 0.005$, $v_{beam} = 2000v_e$, $T_{\perp} = T_e$. The ions are cold. Normalization is in terms

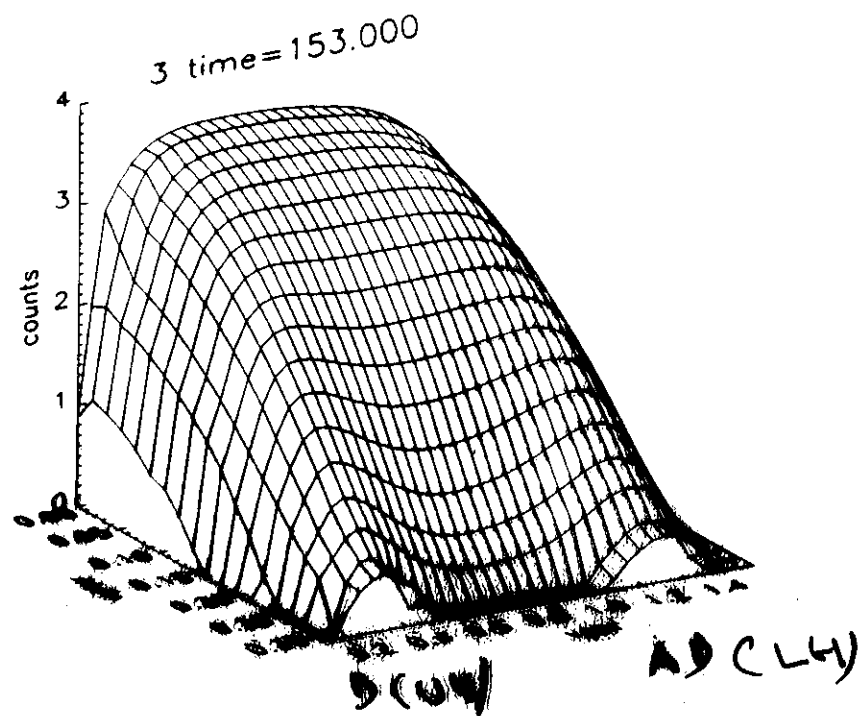
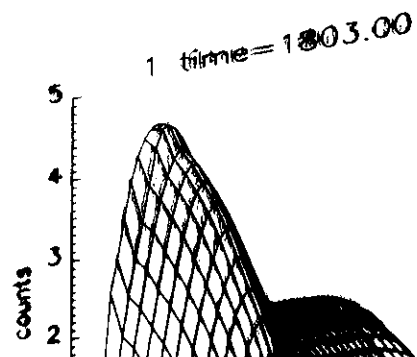
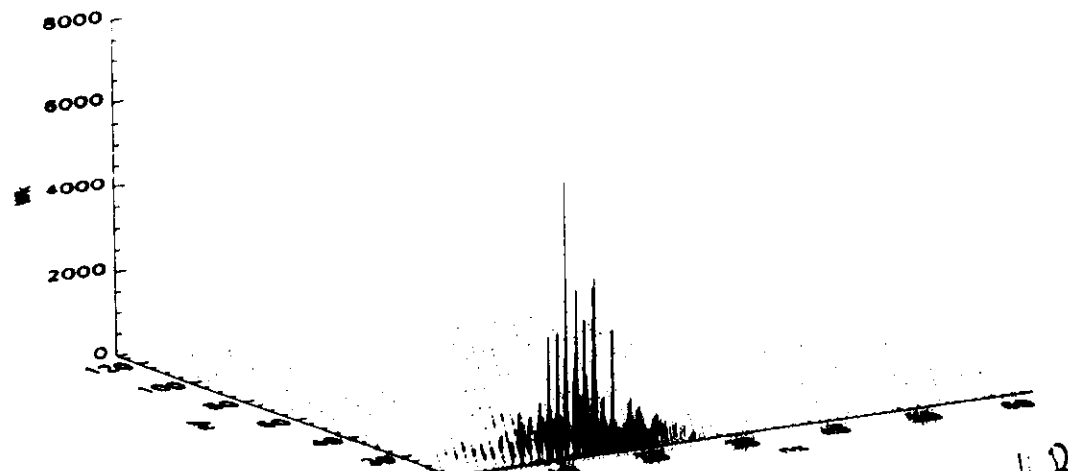


Fig. 3 Dens. distribution with anomalous Doppler Effect at large velocities and the normal Doppler effect at small velocities due to the simultaneous excitation of the lower and upper hybrid branches.

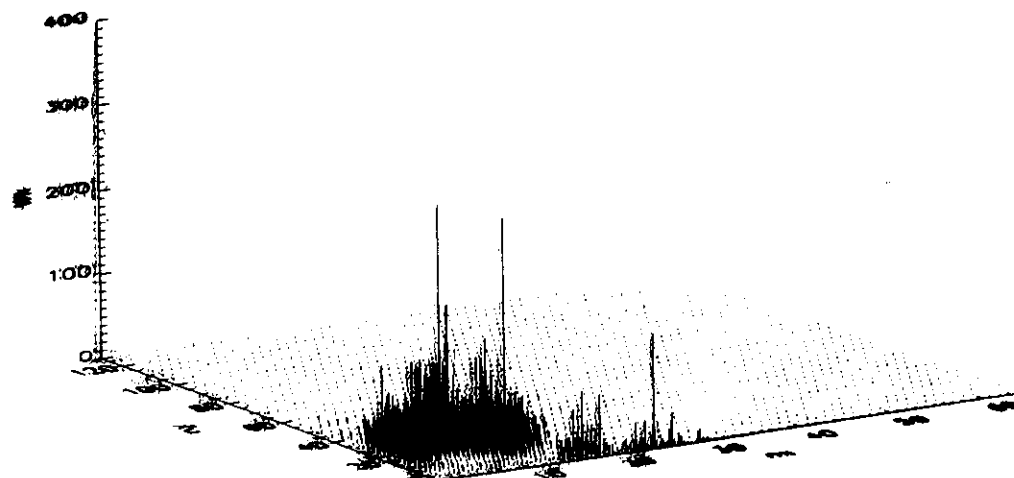


SPECTR 78.0



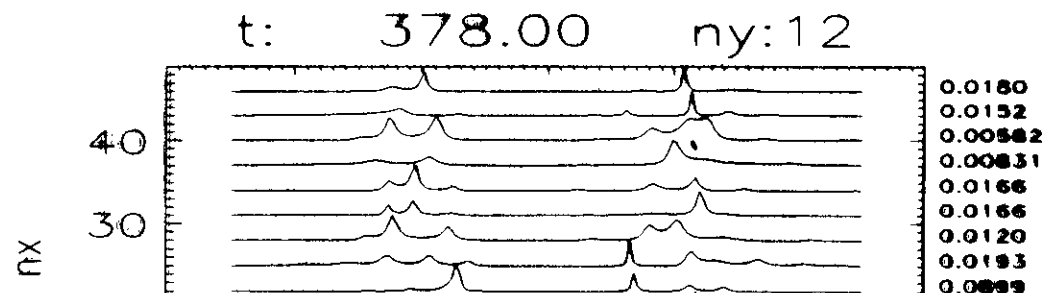
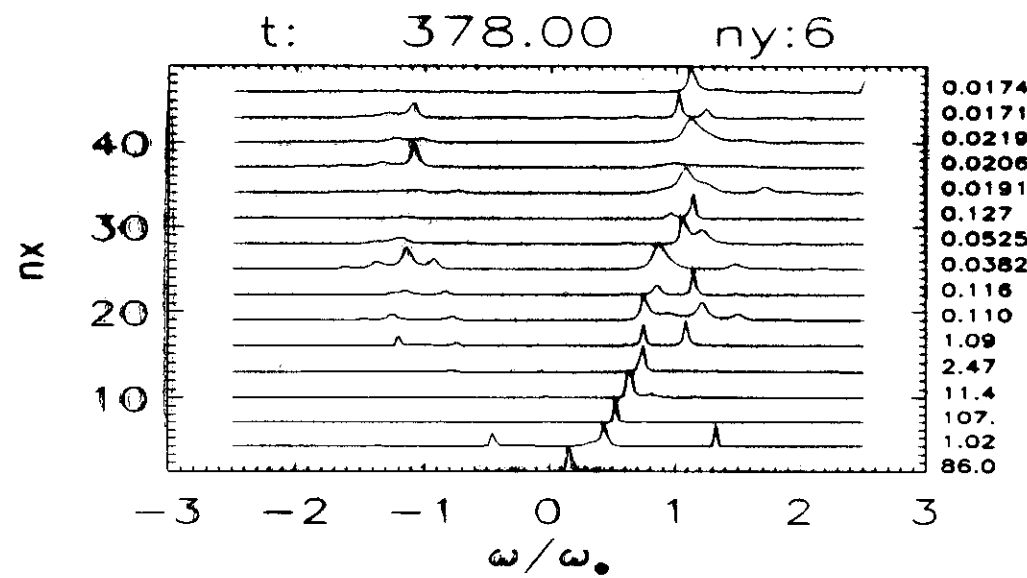
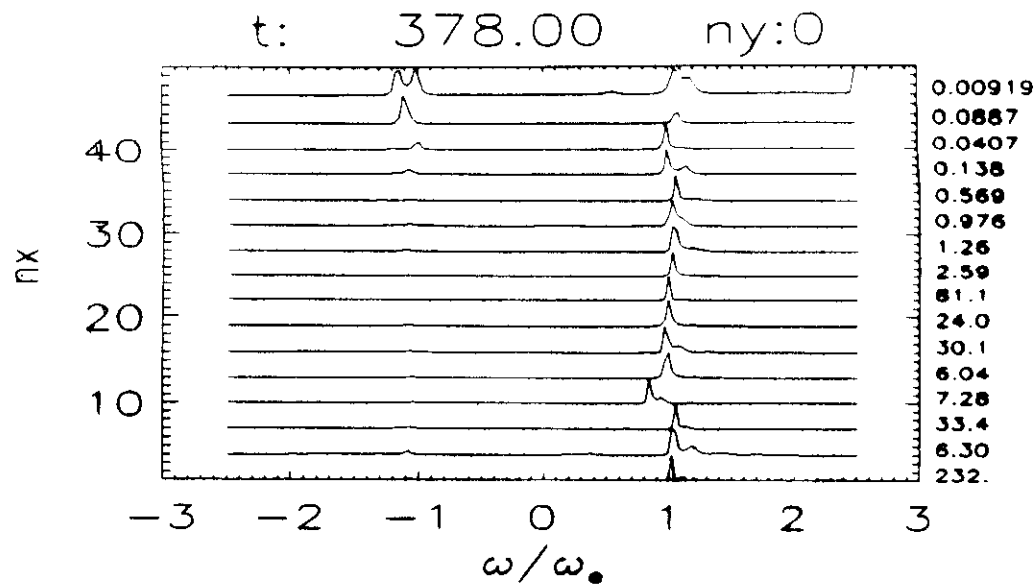
13

SPECTR 453.0



SPECTR 1003.0





3 time=3017.60

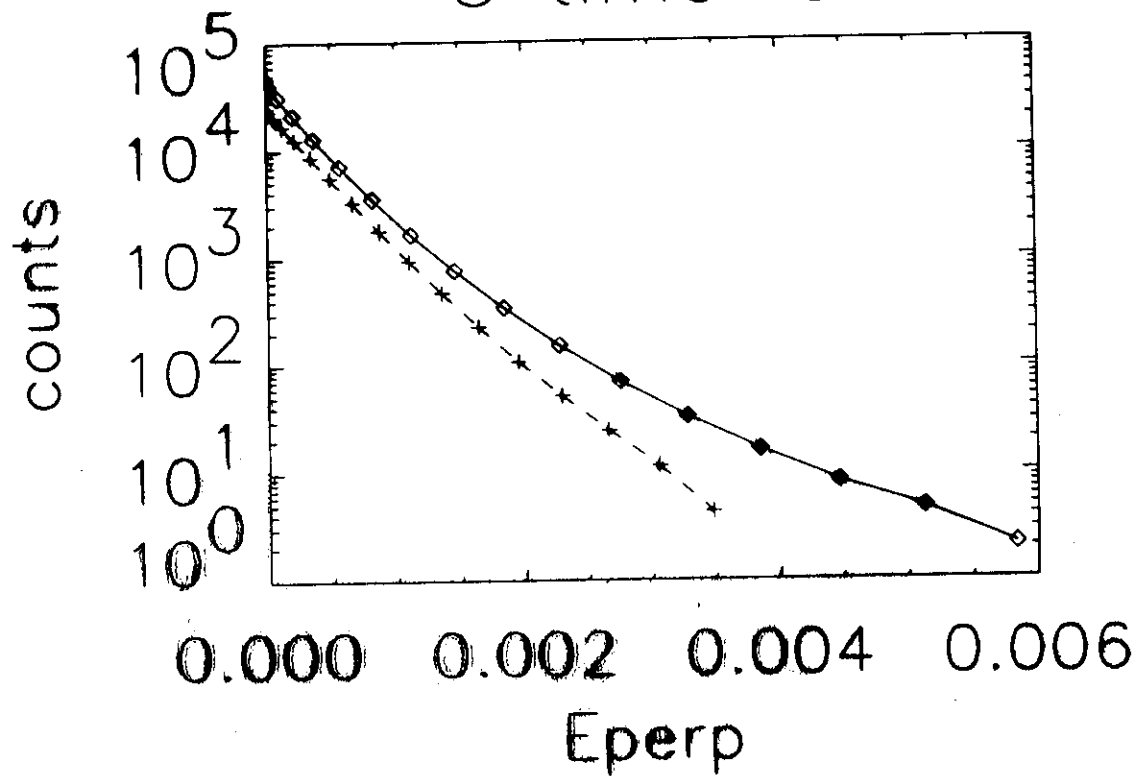
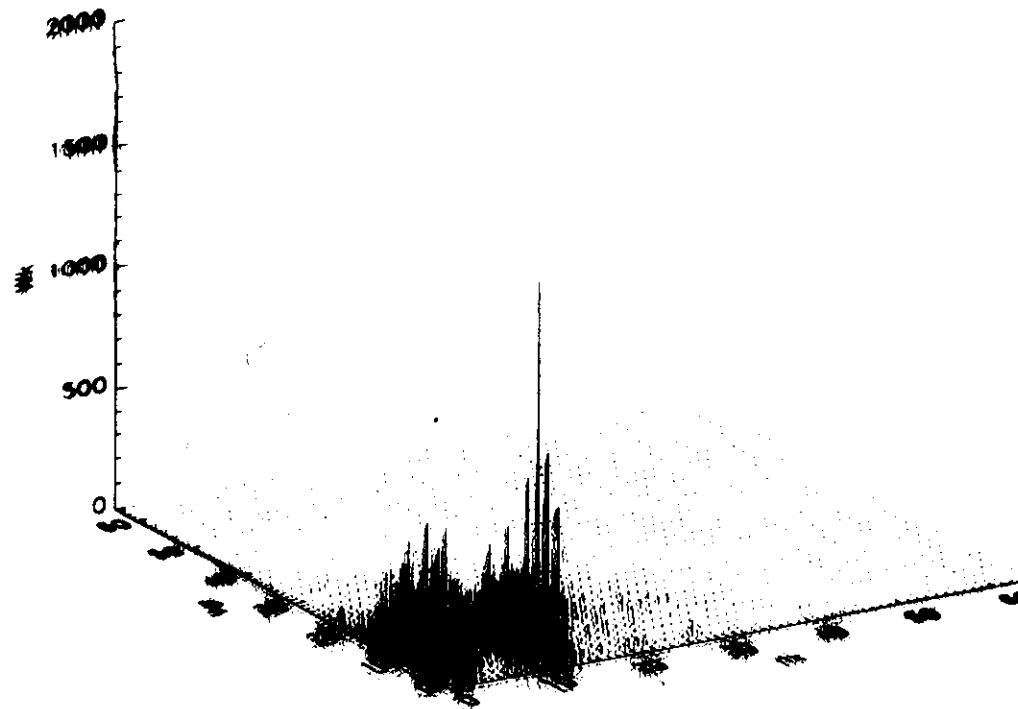
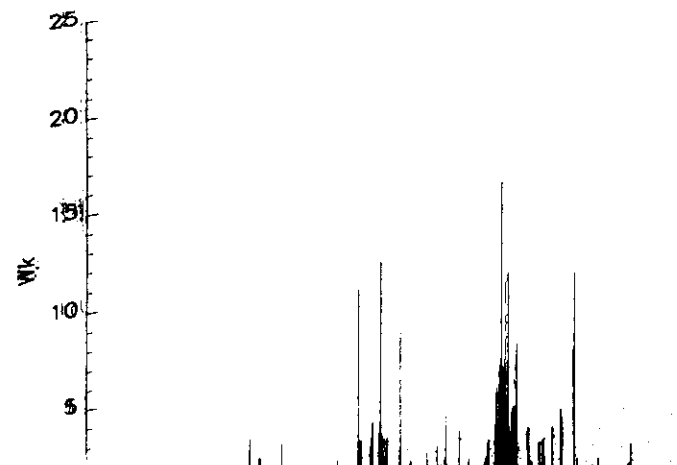


Fig. 8 Perpendicular ion energy distribution (energy in units of $m\omega_e^2$) for a run in which only strongly oblique modes can be excited (representing reflection). The magnetic field is tilted out of the simulation plane (at an angle of 84.3 degrees with x axis). $\Omega_e/\omega_e = 1.8$, $n_b/n = 0.02$, $v_b/u = 0.1$, $v_e/u = 0.06$, $v_i/u = 0.012$, $M/m = 100$. The times $\omega_{\text{et}} = 777, 3017$ are shown.

SPECTR 777.5999



SPECTR 30117.5



Conclusions

Extensive parameter studies have been carried out for the electron driven hybrid modes in a magnetized plasma.

• Linear instability theory:

The lower and upper hybrid branch can be excited simultaneously by an electron beam, resulting in waves which are also separated in wave number space.

Resonant interaction with ions is observed at best.

• Particle simulation results (one-dimensional particle and two-dimensional wave calculations) confirm features of the linear theory. Evolution appears to proceed in two stages. In the first stage the beam drifts the parallel velocity and the wave amplitude increases in plateau and in a second stage the parallel acceleration and wave evolution proceed by the Doppler effect. For modest drifts acceleration of particles from the electron bulk is significant. Perpendicular acceleration of bulk particles can arise from the Doppler effect associated with upper hybrid waves.

short wavelength and may also be associated with SAH waves since strong structure at the hydrogen gyrofrequency was not observed.

4. TOPAZ 2 OBSERVATIONS

The sounding rocket payload TOPAZ 2 was launched from Poker Flat, Alaska, on January 19, 1968, to an altitude of 927 km during an auroral substorm. The substorm began as a bowshock overhead which rapidly moved northward and then stopped at the apogee foot point. The arcs continued to be active but relatively stationary until the payload arrived about 10 minutes later. The payload contained pitch angle scanning electron and ion analyzers, a thermal ion mass spectrometer, and a VLF receiver employing a 5.5-m double-disk antenna. There was a rich variety of plasma phenomena during this flight, including large quasi-stationary electric fields, up to 300 mV/m, electron current density maxima, amplitudes up to 700 eV, and discrete field boundary signatures of auroral layers [Kintner et al., 1970]. In addition, three auroras were observed simultaneously at different altitudes during the flight.

In Figures 11 and 12 we present VLF power spectra

observed during the high-altitude portion of the flight. The power spectrum was measured near apogee when the payload was nearest the most intense auroral arcs. In Figure 11 the power spectrum altitude increases about 15 dB at 2 kHz, which we assume to be the lower hybrid frequency. Structure at the hydrogen gyrofrequency is evident between 2 kHz and 7 kHz. For high frequencies the spectrum appears to be a typical auroral hiss spectrum. In Figure 12 an expanded view of the power spectrum between 3 kHz and 6 kHz is presented along with markers at multiples of the hydrogen gyrofrequency (f_{H+}). Clearly the structure appears to be ordered by f_{H+} with apparent "holes" near multiples of f_{H+} . These features were observed continuously for about 500 s during the flight. We conclude from these results that the wave phenomenon observed during the magnetic substorm (described in the previous section) was also observed during the TOPAZ 2 experiment.

In the next few sections we wish to establish the physical mechanism for the auroral hiss. TOPAZ 2 carried a VLF receiver which was located only 50 cm from the search coil and thereby suffered from pick-up noise and magnetic interference (EMI). Nevertheless, it was possible to determine if a magnetic resonance was present in the SAH waves. Figure 13 shows the VLF power spectrum taken early in the flight at an altitude below 500 km. This appears to be the characteristic auroral hiss spectrum with a peak at the lower hybrid frequency, roughly 6 kHz, and power decreasing with altitude up 100 km. Figure 14 contains the simultaneous magnetic power spectrum. In addition, a background magnetic spectrum measured during the quiet portion of the flight is also plotted to indicate the instrument sensitivity in the presence of EMI. The narrow emission lines are produced by EMI. The simultaneous magnetic spectrum was a broad VLF emission peaking at 9 kHz in agreement with the broad peak in the electric spectrum, also near 9 kHz. However, the sharp peak at 6 kHz in the electric spectrum is absent from the magnetic spectrum. We conclude that the electric peak at 6 kHz was produced by wave power on the electromagnetic lower hybrid resonance cone to which the search coil was not sensitive. On the other hand the search coil was sensitive to the magnetic component of the whistler mode auroral hiss not on the LHR cone which exhibited a broad peak with a maximum near 9 kHz. From the data in Figures 13 and 14 we conclude that electric and magnetic sensors are operating properly and responding consistently to auroral hiss.

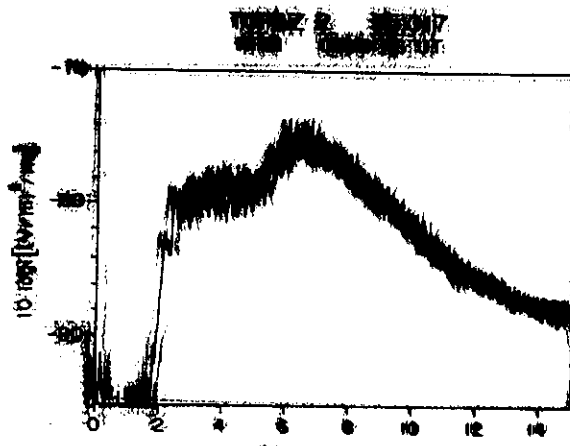


Fig. 11. Auroral VLF power spectrum near 927 km altitude within an auroral arc.

TOPAZ 2 35.017
HF21 0849:46 UT

qualitatively described by (8). We see in Figures 1b and 1c that increasing the H⁺ temperature allows Bernstein modes at higher harmonics to connect with the lower hybrid mode.

Figure 2 shows the effects of varying the value of k_{\parallel} on the structure of the wave modes. In all cases the H⁺ temperature is 0.5 eV. For the case $k_{\parallel} = 0$ we obtain the classical pure Bernstein modes [Chen, 1984]. As is predicted by (8) for $k_{\parallel} = 0$, the frequency shift is positive above ω_{LH} and negative below. In Figures 2b and c, we note the connections of the lower hybrid and Bernstein modes at values of finite k_{\parallel} as roughly predicted by (10). We note in Figure 2c that our numerical calculations show that electron Landau damping is becoming significant at this value of k_{\parallel} .

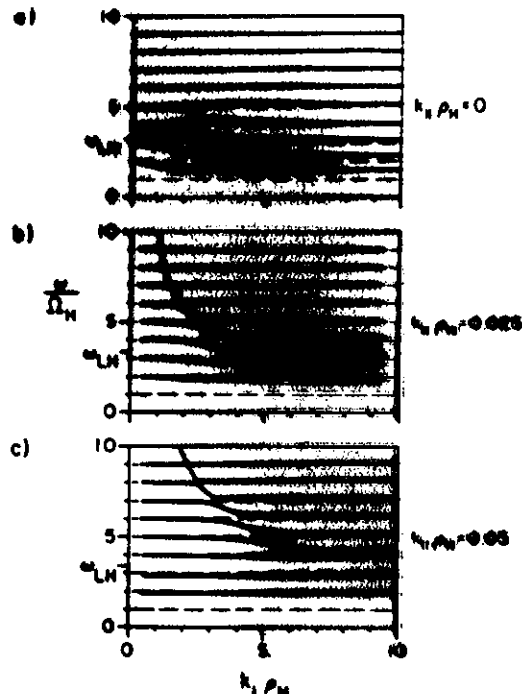


Fig. 2. Dispersion relations of ω_r/Ω_{H0} versus $k_{\perp}\rho_H$ for the different values (a) $k_{\parallel}\rho_H = 0$, (b) $k_{\parallel}\rho_H = 0.025$, and (c) $k_{\parallel}\rho_H = 0.05$. The parameters are $\Omega_{pe} = T_{ce} = T_e = 0.5$ eV, $n_e = 5.5 \times 10^{13}$ cm⁻³, $n_{H0} = 5.0 \times 10^{13}$ cm⁻³, and $\epsilon_0 = 0.25$ eV cm.

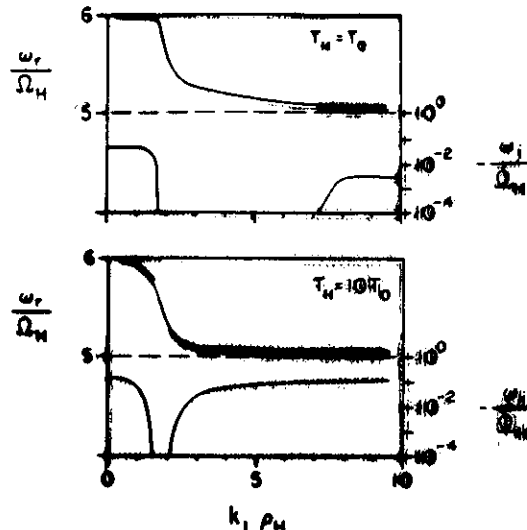


Fig. 3. H⁺ cyclotron damping of wave modes between 5 and 6 GHz shown in Figures 1b and 1c with varying T_H .

$$\chi_b \equiv i \left(\frac{\pi}{2} \right)^{1/2} \frac{\omega_b^2 (\omega - k_{\parallel} v_d)}{k_{\parallel}^2 k_{\perp} v_b} \exp \left\{ - \frac{1}{2} \left(\frac{\omega - k_{\parallel} v_d}{k_{\parallel} v_b} \right)^2 \right\} \quad (11)$$

Here all of the notation is the same as in (2) with the beam drift velocity denoted by v_d . Waves will be driven unstable when their parallel phase velocity is near the beam velocity, i.e., $\omega_r/k_{\parallel} \sim v_d$.

Figure 4 shows the linear growth rate as a function of frequency for $k_{\parallel}\rho_H = 0.05$. The electron beam density is 1% of the background electron density, and the drift energy is 250 eV. In this case the H⁺ temperature is 5 eV, and the O⁺ temperature is 0.5 eV. We clearly see that the bulk in wave growth comes from the thermal H⁺ in the background plasma. Also, these bulk occur in the harmonic bands just above the lower hybrid frequency, ω_{LH} .

In summary, we have considered the effects of thermal H⁺ on the lower hybrid mode at frequencies near the lower hybrid resonance frequency. We have shown that inclusion of H⁺ of only eV energies may cause waves to be damped near the H⁺ gyrofrequency frequencies above ω_{LH} . This is ultimately due to the conversion process between the lower hybrid and

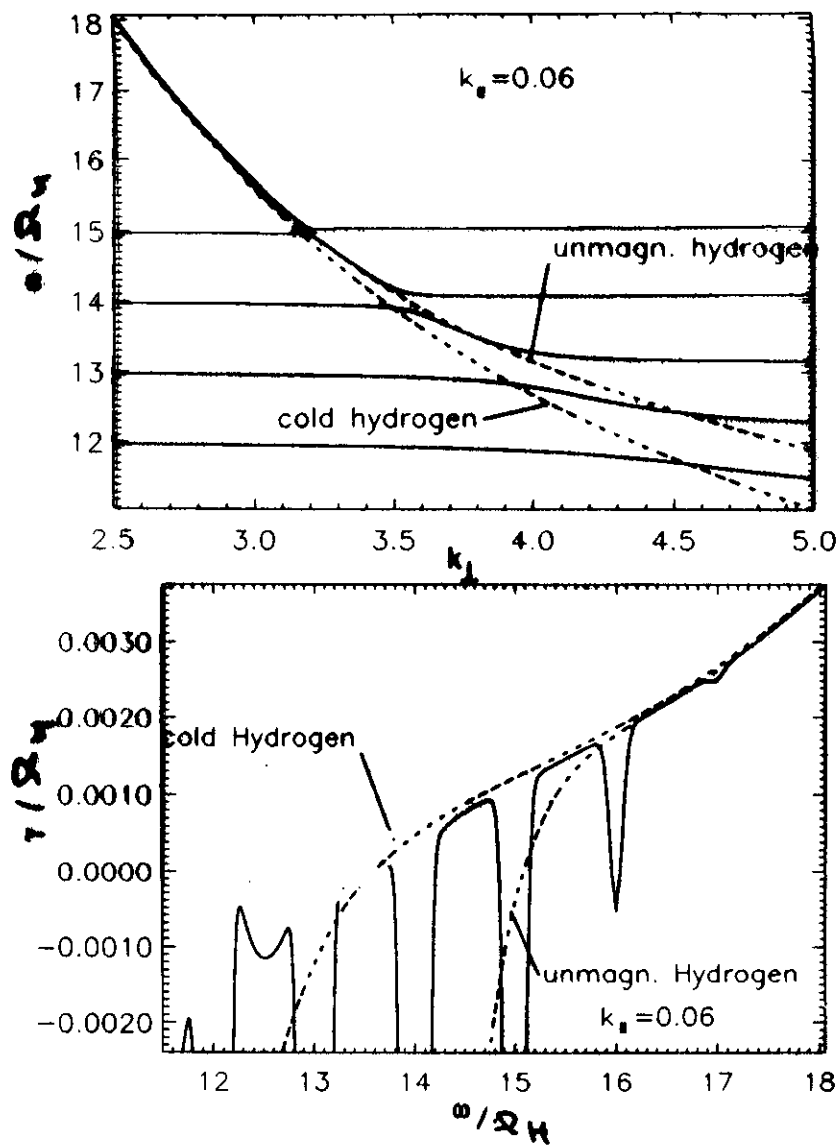
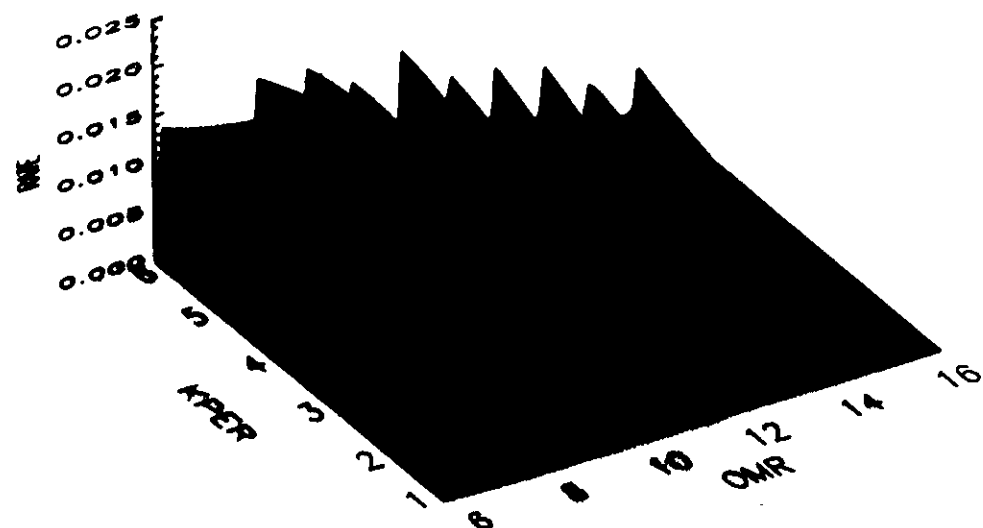
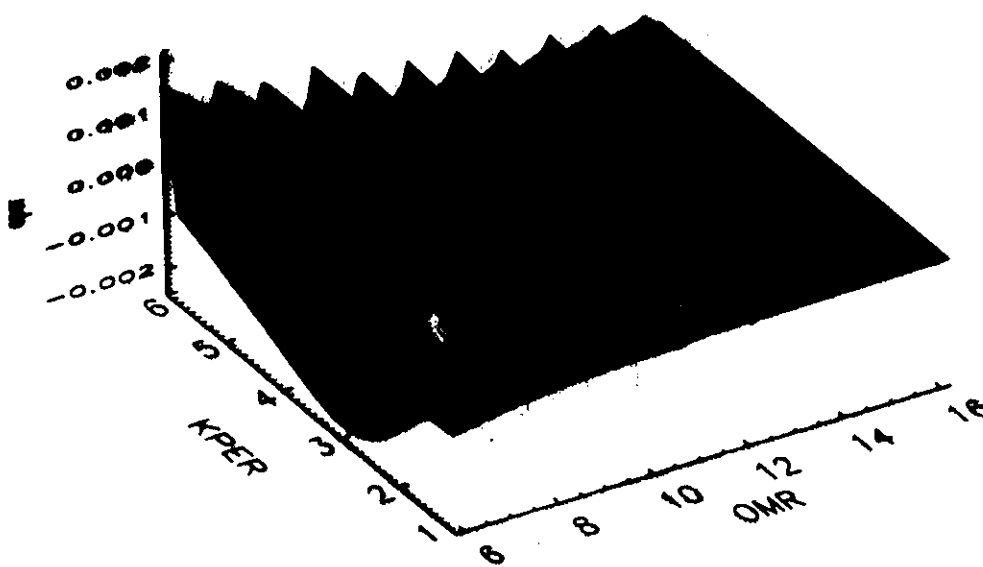


Figure 2. a. Dispersion relation for a oxygen-hydrogen plasma with $\omega_e/\omega_{ce} = 0.4$, $n_H/n_e = 0.1$, $T_e = T_O = T_H$, $k_\parallel = 0.06$; Approximations using cold hydrogen and unmagnetized kinetic hydrogen are also shown



$\frac{d^2}{dK^2} > 0$



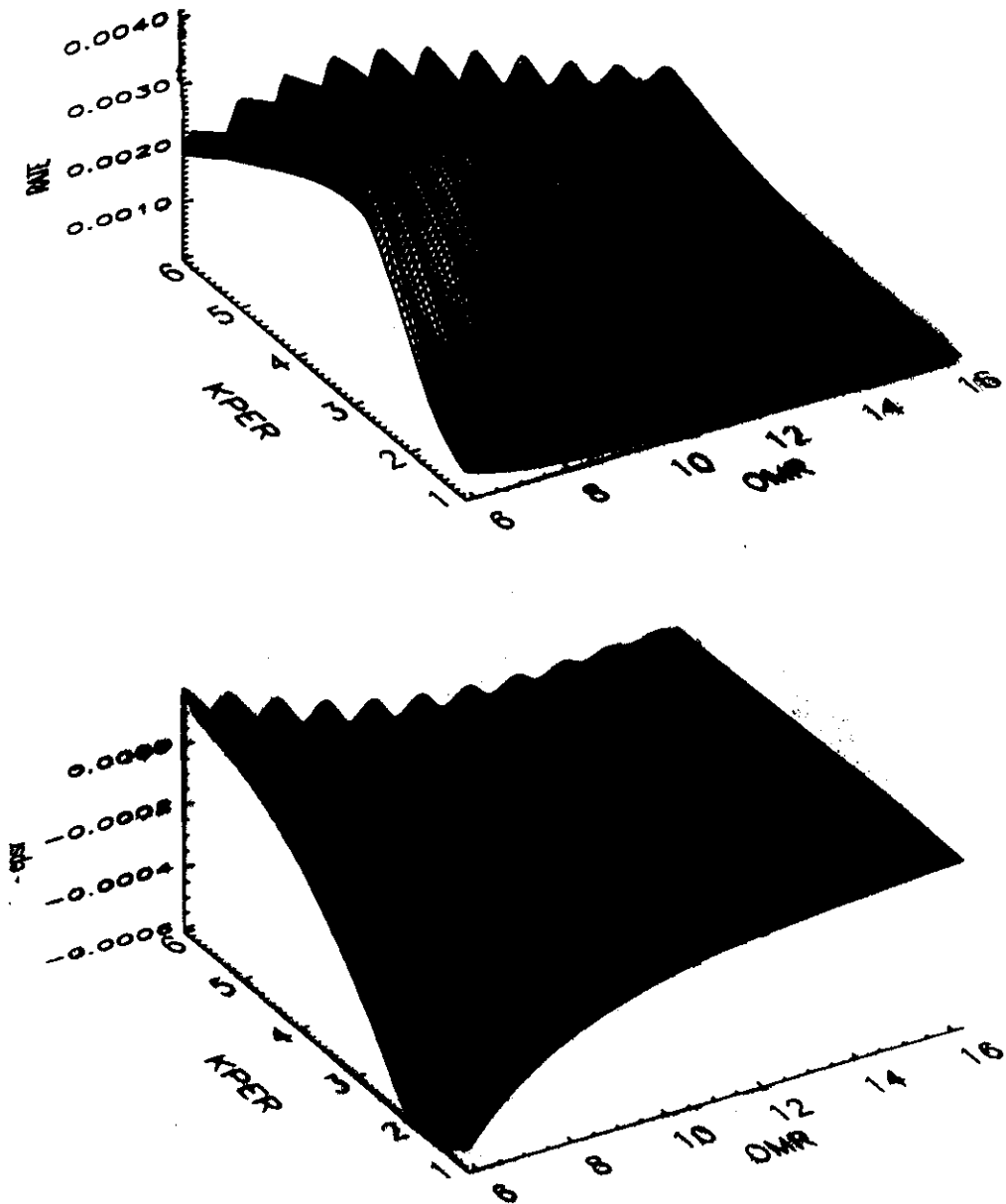


Figure 3. Hydrogen heating rate and real part of susceptibility for

Conclusions

1. Ion Heating

req. Kinetic theory of
magnetized Plasma

cyclotron resonance absorption

$$\omega \rightarrow n\omega_H, \quad k_{\perp} T$$

propagation effects in
in homogen. plasma $n(x), B(x)$

2) k, ω range restricted by
Landau damping on electron
bulk + medium energy components
(secondary electrons)

3) destabilization by
electron beam Landau damping

$$\gamma \ll \gamma_{max}$$

propagation
 $\propto (k \times v_s)^{-1}$

4) - - - - -